CHEMISTRY OF MATERIALS
Cite This: Chem. Mater. 2018, 30, 1209−1217
Article
pubs.acs.org/cm

Dopant Distribution in Atomic Layer Deposited ZnO:Al Films Visualized by Transmission Electron Microscopy and Atom Probe Tomography

Yizhi Wu,[†] A. Devin Giddings,[‡] Marcel A. Verheijen,[†] Bart Macco,[†] Ty J. Prosa,[‡] David J. Larson,[‡] Fred Roozeboom,[†,§] and Wilhelmus M. M. Kessels*[,†]

[†]Eindhoven University of Technology, P.O. Box 513, 5600 MB Eindhoven, The Netherlands
[‡]CAMECA Instruments Inc., 5500 Nobel Drive, Madison, Wisconsin 53711, United States
[§]Holst Centre, P.O. Box 8550, 5605 KN Eindhoven, The Netherlands

Supporting Information

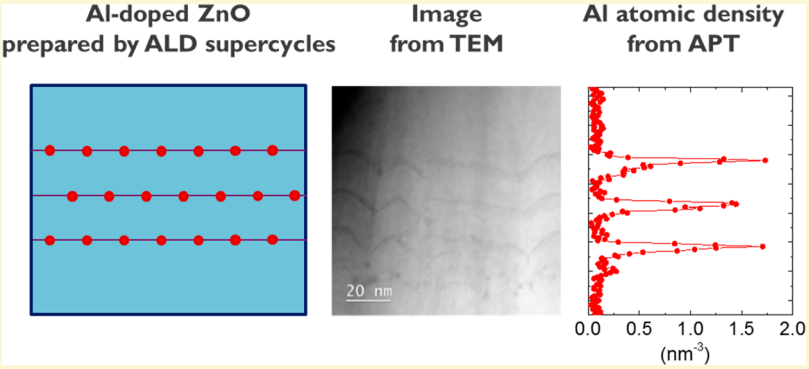

ABSTRACT: The maximum conductivity achievable in Al-doped ZnO thin films prepared by atomic layer deposition (ALD) is limited by the low doping efficiency of Al. To better understand the limiting factors for the doping efficiency, the three-dimensional distribution of Al atoms in the ZnO host material matrix has been examined on the atomic scale using a combination of high-resolution transmission electron microscopy (TEM) and atom probe tomography (APT). Although the Al distribution in ZnO films prepared by so-called "ALD supercycles" is often presented as atomically flat δ-doped layers, in reality a broadening of the Al-dopant layers is observed with a full-width−half-maximum of ∼2 nm. In addition, an enrichment of the Al at grain boundaries is observed. The low doping efficiency for local Al densities > ∼1 nm^{-3} can be ascribed to the Al solubility limit in ZnO and to the suppression of the ionization of Al dopants from adjacent Al donors.

INTRODUCTION

Transparent conducting oxide (TCO) thin films are a class of materials that are commonly used as transparent electrodes in a wide variety of commercial optoelectronic devices, most prominently displays and solar cells.[1−3] The most commonly used TCO is indium tin oxide (ITO). Although this material yields very good optoelectronic properties, widespread use, particularly for large-scale applications, is hampered by the scarcity of indium. Another TCO is ZnO, for which there is an abundant availability of constituent materials, and therefore ZnO has been reported to be a promising, low cost alternative to ITO.[4] However, one key requirement for TCOs in many applications is a film resistivity on the order of 1 mΩ·cm or lower.[5] For ZnO, this can be achieved through cation doping, with Al being the most commonly used dopant. This material is known as Al-doped ZnO, abbreviated as ZnO:Al or AZO.

There are several methods by which ZnO:Al thin films can be prepared, each with their pros and cons. Furthermore, each of these methods results in particular properties of the resultant films. Physical vapor deposition (PVD), in particular sputtering, and chemical vapor deposition (CVD) methods have been most popular, and with these methods resistivity values on the order of 0.1 mΩ·cm have been achieved for ZnO:Al thin films.[5] However, compared to these methods, atomic layer deposition (ALD)[6−10] can provide a number of advantages that are particularly relevant for demanding emerging applications: (*i*) The cyclic nature of ALD allows accurate control of film thickness even for ultrathin films. (*ii*) ALD offers excellent uniformity, necessary for large area applications. (*iii*) ALD is unique in its ability to cover challenging surface topologies with a very high degree of conformality. (*iv*) The absence of energetic species (ions, neutrals, photons) makes it a "mild" deposition technique, which does not cause damage to the underlying surface.[10,11] (*v*) ALD processes work at relatively low temperatures, making the

Received: August 30, 2017
Revised: February 2, 2018
Published: February 5, 2018

DOI: 10.1021/acs.chemmater.7b03501
Chem. Mater. 2018, 30, 1209−1217

technique suitable for situations where thermal budgets are restricted, and finally, (*vi*) the atomic composition and hence the doping level can, in principle, be accurately controlled in a highly repeatable manner by tuning the ALD cycle ratio between the host matrix and dopant materials.

Despite the advantages of growing ZnO:Al thin films by ALD, the improvement in resistivity by Al doping is still limited. For example, in previous work using the commonly applied trimethyl aluminum precursor (TMA, $[Al(CH_3)_3]_2$),[12] it was shown that by varying the Al doping level (defined as the proportion of Zn atoms replaced by Al; see below), the resistivity could be improved from 9.8 mΩ·cm to 2.2 mΩ·cm. However, this is still not sufficient to meet the required performance target of <1 mΩ·cm. Furthermore, the doping efficiency, i.e., the percentage of Al atoms that act as active dopants, releasing free electrons, is generally lower than 10%. The inactive Al atoms can act as scattering centers rather than contributing to the number of free electrons. This will have a negative effect on the carrier mobility and hence on the electrical transport in the ZnO:Al films.

The limited improvement in conductivity and the low doping efficiency of ALD-ZnO:Al have been attributed as principally being due to the inhomogeneous distribution of the Al atoms in ZnO:Al films, originating from the so-called "supercycle" growth mode.[8,12,13] As shown in Figure 1a, one supercycle consists of *m* ZnO cycles and one Al_2O_3 cycle, where *m* is called the cycle ratio. By modifying this cycle ratio, the doping level can be tuned. The targeted film thickness can be achieved by repeating a certain number *N* of these supercycles. Such a growth mode can lead to a lamellar distribution of Al atoms in the ZnO:Al films, as shown schematically (and idealized) in Figure 1b. To increase the Al doping level, the cycle ratio *m* is lowered, which will correspondingly decrease the spacing, *l*, between the adjacent Al-dopant layers. Our previous work revealed two distinct regimes for ZnO:Al films prepared as a function of cycle ratio *m*. It was shown that the doping efficiency is approximately constant when the spacing *l* of adjacent Al-dopant layers is higher than a critical value of l_c = 3.8 nm, which corresponds to a doping level of 6.9%.[12] In this region, the resistivity decreases with increasing cycle ratio *m*. For $l < l_c$, the doping efficiency drops and the resistivity increases with *m*. Such a correlation between the doping efficiency and the spacing *l* has also been observed by Lee et al.,[8] who reported that l_c ranged from 2.3 to 2.6 nm for their films.

When correlating the doping efficiency with the spacing between the Al-dopant layers, it should be realized that the spacing only describes the dopant distribution in the growth direction. The areal density of Al atoms within each individual Al-dopant layer can also play a role. There have been two experimental studies that support this, showing that by increasing the lateral distance of Al atoms in the Al-dopant layers, the doping efficiency can be increased and the film resistivity can be lowered.[13,14] In one of these studies, the number of Al atoms incorporated in one ALD cycle was reduced by deactivating a fraction of the surface functional groups on which TMA molecules can chemisorb. The deactivation took place by using ethanol as a reactant before the dosing step of TMA. This approach improved the doping efficiency by a factor of ~2.[13] In another approach dimethylaluminum isopropoxide (DMAI, $[Al(CH_3)_2(\mu\text{-}O^iPr)]_2$) was selected as an alternative Al precursor to TMA.[14] Due to steric hindrance of the larger O^iPr ligand, the number of Al atoms deposited per Al_2O_3 cycle was significantly reduced from 11.0 to 2.9 nm^{-2}. As a result, a higher doping efficiency of 50−60% compared to <10% for TMA and a lower

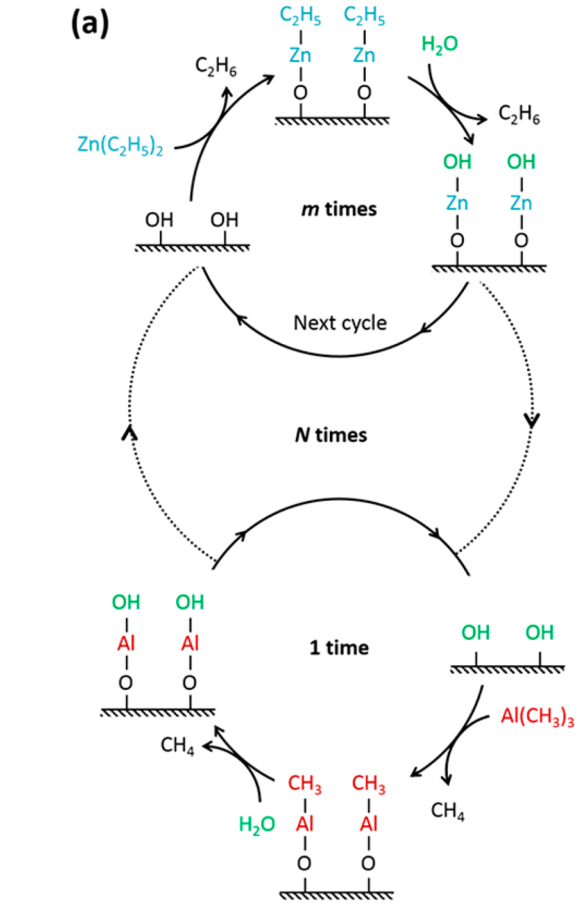

Figure 1. (a) Schematic representation of one ALD supercycle for the preparation of ZnO:Al films. One supercycle, carried out *N* times, consists of *m* cycles of ZnO and one cycle of Al_2O_3, where *m* is called the cycle ratio. One individual ZnO or Al_2O_3 ALD cycle consists of four steps: precursor dosing/purge/coreactant dosing/purge. Diethylzinc (DEZ), trimethylaluminum (TMA), and deionized water vapor serve as the Zn precursor, Al precursor, and coreactant, respectively. (b) Schematic and idealized representation of a ZnO:Al film prepared by repeating *N* ALD supercycles as shown in a. The Al dopant atoms are indicated assuming an idealized δ-function distribution. The vertical spacing *l* between adjacent dopant layers is determined by the cycle ratio *m*. The lateral spacing between dopants is *d*.

resistivity of 0.7 mΩ·cm compared to 2.4 mΩ·cm for TMA was achieved.[11,14] A similar effect was achieved for ZnO:B using the relatively large precursor triisopropyl borate (TIB, $[B(O^iPr)]_3$) for B doping.[15]

Obviously, the doping level and the doping efficiency of Al-doped ZnO films prepared by ALD are important factors determining the performance of the films for TCO applications,

DOI: 10.1021/acs.chemmater.7b03501
Chem. Mater. 2018, 30, 1209−1217

Table 1. Properties of the ZnO:Al Films with Thicknesses of 40 ± 2 nm As Studied by APT and TEM[a]

	growth parameters			doping level	electrical properties			
layer	supercycles N	cycle ratio m	spacing l (nm)	Al fraction AF_{global} (%)	resistivity ρ (mΩ·cm)	carrier density n_e (10^{20} cm^{-3})	mobility μ (cm^2 V^{-1} s^{-1})	doping efficiency η (%)
AZO-1	3	85	13.7	1.9	5.1	1.1	10.8	7.1
AZO-2	11	23	3.8	6.9	2.4	3.0	8.7	8.7
AZO-3	19	12	2.0	16.4	4.9	3.7	3.5	4.7

[a]The films have been selected as typical representatives of ZnO:Al films with lowly-doped (AZO-1), optimally-doped (AZO-2), and highly-doped (AZO-3) Al doping levels.[12] The spacing l indicates the vertical distance between adjacent AlOx layers. The doping level in the ZnO:Al films is characterized by the Al fraction in the films as measured by XPS.[12] The electrical properties were measured for films deposited on p-Si wafers with 450 nm thermal oxide.[12]

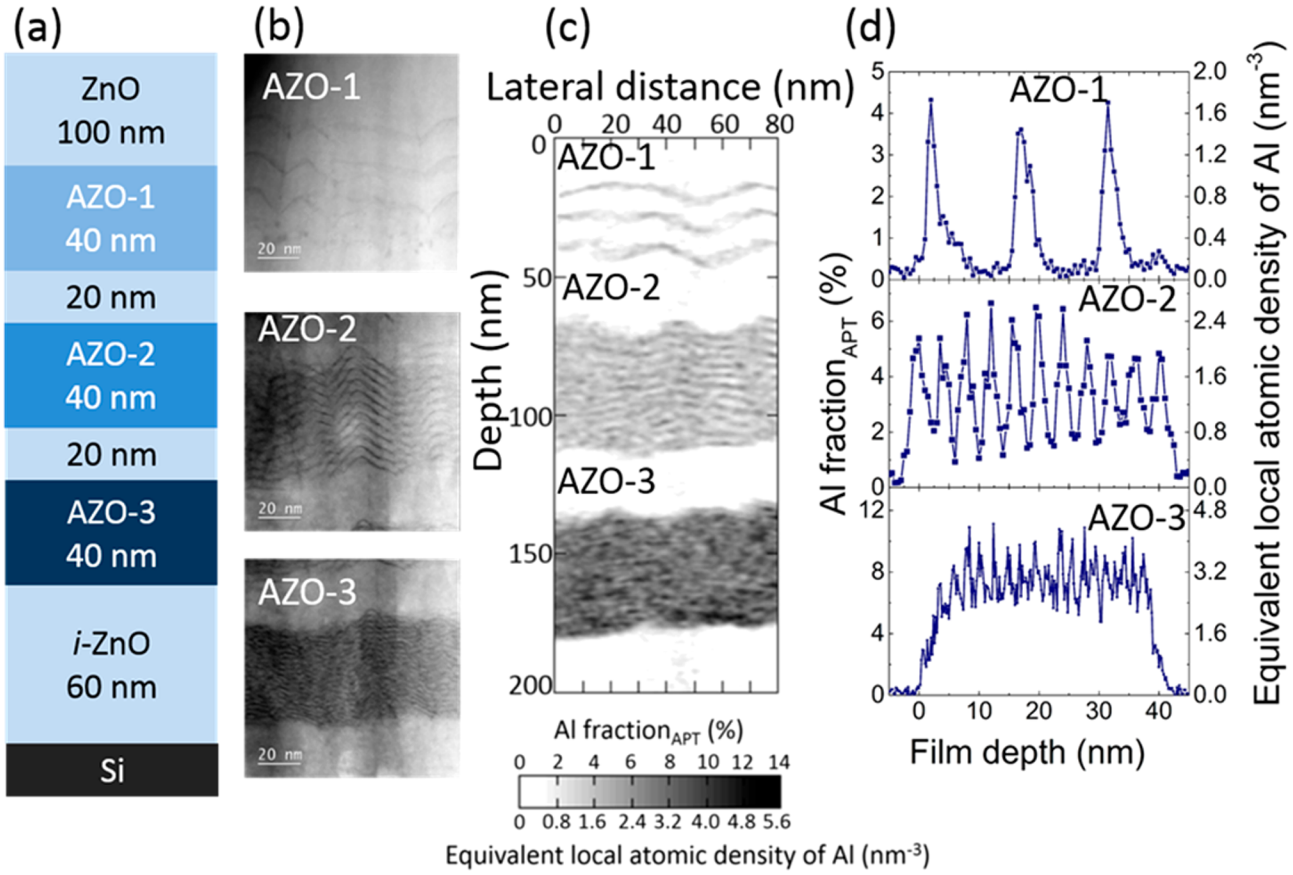

Figure 2. (a) Schematic representation of the structure of the ZnO/ZnO:Al film stack prepared on a Si substrate and on a microtip coupon for TEM and APT analysis, respectively. (b) High-resolution HAADF-STEM images of the three ZnO:Al films. (c) Two-dimensional depth profile of the Al fraction measured by APT showing the Al distribution in the film stack for a projected volume with a depth of 5 nm. (d) One-dimensional local depth profile of the Al fraction in the three ZnO:Al films measured by APT. These profiles are extracted from a cylindrical subvolume with a diameter of 15−20 nm from a region carefully selected (avoiding grain boundaries) in which the interface between the ZnO matrix and the Al-dopant layers are approximately locally flat and oriented normally to the sampling direction.

and they depend largely on how the Al-dopant atoms in the films are distributed. The conventional view that the Al atoms are concentrated only at distinct film depths in a perfect arrangement (as illustrated in Figure 1b)—a so-called δ-doping profile—is clearly an oversimplification. The Al-dopant layers might be broadened by intermixing effects and by the influence of surface roughness, while also the occurrence of grain boundaries in the polycrystalline matrix can play a role. Therefore, in this work, we investigate the distribution of Al atoms in ZnO:Al and discuss how this distribution affects the doping efficiency. To do so, we prepared ZnO:Al thin films by ALD using the conventional Al precursor TMA in the supercycle growth mode. The spatial distribution of the Al atoms was obtained at an atomic resolution by transmission electron microscopy (TEM) and atom probe tomography (APT). The latter is a tool for 3D imaging of the composition of thin films at the atomic scale, which is found to be particularly powerful for doped films.[16−19]

EXPERIMENTAL SECTION

Intrinsic and Al-doped ZnO films were prepared using an Oxford Instruments OpAL ALD reactor at a substrate temperature of 250 °C. Diethylzinc (DEZ, $Zn(C_2H_5)_2$), TMA, and deionized water vapor were used as precursors.[12] From our previous work,[12] we have identified the supercycle conditions to grow the three types of ZnO:Al films that can be representatively labeled as lowly, optimally, and highly doped films. Table 1 describes the growth parameters used to create the three conditions as well as the resulting electrical properties. The number of

DOI: 10.1021/acs.chemmater.7b03501
Chem. Mater. 2018, 30, 1209−1217

supercycles, N, is the number of Al_2O_3 ALD cycles used in each film's deposition. These values are 3 (lowly doped), 11 (optimally doped), and 19 (highly doped), respectively, for the films denoted AZO-1 to AZO-3. Earlier, we reported that a minimum resistivity of 2.4 mΩ·cm was obtained for the optimally doped case AZO-2. For comparison, the low doping in AZO-1 results in a lower carrier density, while the high doping in film AZO-3 leads to a lower carrier mobility.

In Table 1, the doping level is presented by the aluminum fraction (AF), which represents the fraction of Zn atoms replaced by Al atoms in the ZnO:Al film. The value of AF is given by

$$\mathrm{AF} = \frac{[\mathrm{Al}]}{[\mathrm{Al}] + [\mathrm{Zn}]} \quad (1)$$

The atomic percentages of Zn and Al were measured either by X-ray photoelectron spectroscopy (XPS), denoted as AF_{global}, or by APT, denoted as AF_{local}. Note that AF_{global} represents the averaged Al doping level throughout an entire ZnO:Al film, while AF_{local} represents an Al doping level of a selected nanoscale subvolume of the AZO film, extracted from the APT data set.

In this work, a stack was prepared consisting of three ZnO:Al films with a film thickness of 40 ± 2 nm each. The conditions for the ZnO:Al films were identical to those used as the films listed in Table 1. In the stack, the ZnO:Al films were separated and capped by intrinsic ZnO films as shown schematically in Figure 2a. This geometry enabled data collection on all three film types in a single APT and TEM measurement. Within one deposition run, the stack was prepared on both a Si substrate for the TEM measurements and on a commercially available Si microtip array coupon with flat-top Si microtips for the APT measurements. A native oxide was present on both the Si substrate and the Si microtip array coupon.

As mentioned, the complete stack also contained a ZnO capping film and ZnO buffer films between the three ZnO:Al films of interest. The top 100 nm ZnO cap film served two purposes: (*i*) during focused ion beam (FIB) milling, it was used as a sacrificial film to protect the ZnO:Al films from ion implantation, which could damage the structure, and (*ii*) it provided sufficient material for the apex of the APT specimen needles to reach an equilibrium shape during the initial stages of field evaporation, before the film of interest was reached. The two 20-nm-thick ZnO buffer films grown between the ZnO:Al films were intended (*i*) to clearly separate ZnO:Al films for the TEM and APT imaging and data collection and (*ii*) to allow the APT specimen apex to return to an equilibrium shape between each ZnO:Al film. This prevented changes of the specimen's equilibrium tip shape, expected to occur during field evaporation of one film, from influencing the measured geometry of the next. The 60 nm *i*-ZnO film at the bottom was deposited to provide sufficient material so that the third ZnO:Al film could be completely evaporated before the field evaporation of the APT specimen reaches the Si substrate layer.

The flat-top Si microtips upon which the deposition was made had an initial diameter of ∼2 μm.[20] After the ALD coating, they were prepared using standard FIB annular milling protocols[21,22] into APT specimen needles with an initial diameter of ∼50 nm and half shank angle of ∼15°. By depositing directly onto the microtip coupon, the APT specimens could be prepared with reduced FIB requirements since no lamella lift-out was necessary. High resolution SEM images of the specimen needles were taken before APT measurement and, when possible, after the measurement to provide geometric information to assist with the data reconstruction. Deposition onto presharpened microtips[20] with an initial diameter ∼10 nm was also prototyped, but this proved inferior to using the flat-top type. The APT measurements were performed in CAMECA LEAP 4000X microscopes[23] with the specimen at a temperature of 25 K, laser pulse energies between 0.3 pJ and 10 pJ, and laser pulse repetition rates of 160 kHz (reflectron-type system) or 500 kHz (straight-flight path system). Cross-sectional TEM studies on FIB prepared lift-out samples were performed in high-angle annular dark-field (HAADF) STEM and in bright-field TEM modes using a probe-corrected TEM (JEOL JEM ARM 200F) equipped with a 100 mm^2 Centurio SDD detector and a FEI Tecnai F30ST TEM. Note that all results presented were obtained from one APT specimen and one TEM specimen (both deposited in the same run).

RESULTS

Two-Dimensional Depth Profiles. The morphology of the three ZnO:Al films has been imaged by both TEM and APT. The lamellar structures of the ZnO:Al films were imaged in HAADF-STEM mode as shown in Figure 2b. The dark streaks represent the positions of the Al-dopant layers, where Al atoms were incorporated during single Al_2O_3 ALD cycles of the supercycle. Figure 2c shows the two-dimensional (2D) profiles of the Al distribution in the stack, extracted from the 3D APT data. The projected volume for the 2D APT profiles has a depth of 5 nm. The gray scale shading in the 2D APT profiles represents the Al doping levels and is quantified by AF_{local}. Consistent with the TEM images, the gray streaks in Figure 2c indicate the Al-dopant layers. In both cases, rather than being flat, the Al-dopant layers are observed to be ridged. This reflects the faceting of the ZnO:Al polycrystalline[12] grains (grain size is ∼40 nm, see below) obtained for the ALD-prepared films.

The equivalent estimated local atomic density of Al is also indicated in Figure 2c. This parameter is derived from AF_{local} by multiplying AF_{local} with the bulk atomic density of Zn in the undoped ZnO films, which is estimated at 4.0×10^{22} cm^{-3} from our previous work.[12] In both the TEM images and the 2D APT profile, 3 and 11 individual Al-dopant layers can be distinguished in the AZO-1 and AZO-2 films, respectively. These values are consistent with the number of supercycles, N, used to incorporate Al into these two films, as shown in Table 1. The AZO-3 film with $N = 19$ has a lamellar structure that is less clearly resolved in both the TEM (Figure 2b) and the APT profiles (Figure 2c). This can be attributed to the smaller cycle ratio, m, leading to a relatively small spacing between the Al-dopant layers (l = ∼2 nm) as well as to the projection of fine-scale surface roughness on the 2D profiles and the broadening of the Al-dopant layers. The latter will be addressed in the next section.

One-Dimensional Local Depth Profiles. One-dimensional (1D) local depth profiles created from the 3D APT data are presented in Figure 2d. The term "local" is used to emphasize that the profiles are not the projections from the entire 3D data sets shown in Figure 2b but instead are collected from cylindrical subvolumes with a diameter of 15 or 20 nm. The subvolumes are carefully selected from regions within a grain in which the interfaces between the ZnO matrix and the Al-dopant layers were close to being flat for an area with the size of the cylindrical cross-section, for all the dopant layers in the subvolume. The cylindrical subvolumes were oriented to be normal to the interface plane, which, because of the faceting, would not necessarily be parallel to the local growth direction of the film. However, given the scale of the roughness, particularly in the case of layer AZO-2, it must be accepted that it is not possible to have a perfectly positioned analysis subvolume, a factor that will introduce apparent interface broadening into the 1D profiles. Despite this, individual peaks, which represent the Al-dopant layers, are observed in all three ZnO:Al films. Both the number of peaks and the spacing between the peaks are consistent with the conditions and film properties, as listed in Table 1, in particular the number of supercycles, N.

These 1D profiles clearly show that the distribution of Al in the depth direction is not a δ function. Instead, from the full shape of the peaks in the upper profile in Figure 2d, it can be estimated that the peaks have a full-width−half-maximum (fwhm) of ∼2 nm. The Al atoms in a single Al-dopant layer are incorporated

DOI: 10.1021/acs.chemmater.7b03501
Chem. Mater. 2018, 30, 1209−1217

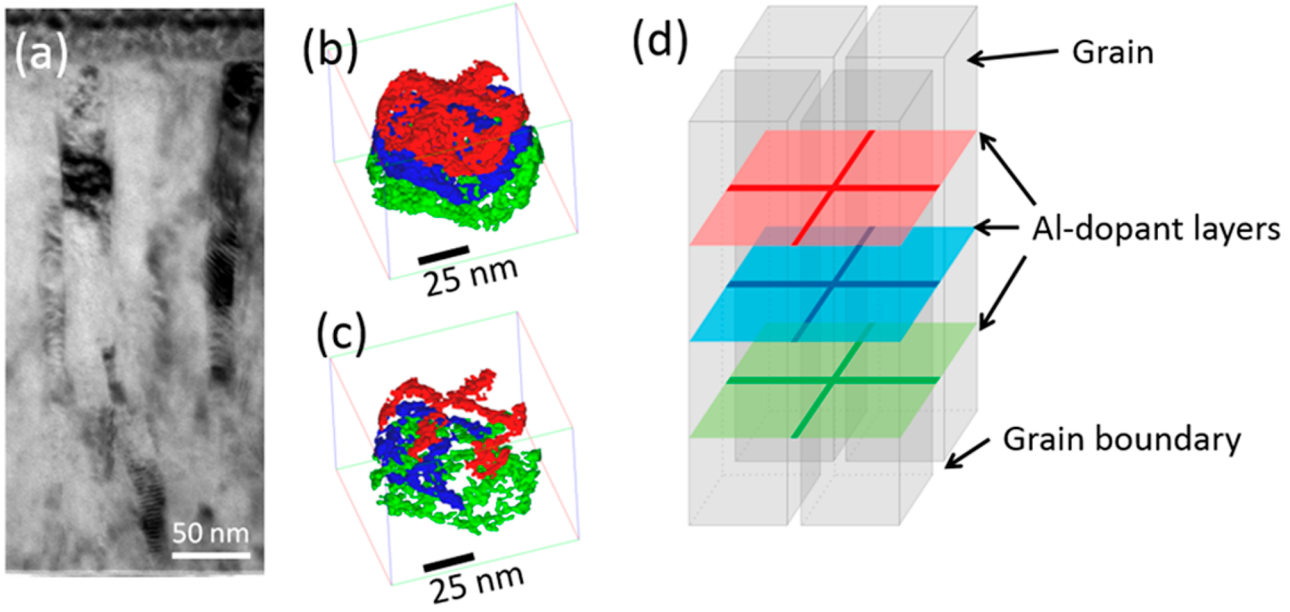

Figure 3. (a) Cross-sectional bright-field TEM image of the entire film stack as schematically shown in Figure 1a. Iso-concentration surfaces created from the APT data set at (b) AF_{local} = 1.7% and (c) AF_{local} = 3.0% in the AZO-1 film. This layer was prepared with three supercycles, as can also be observed from the three Al-dopant layers in the plots (each have been assigned a different color for clarity). (d) Schematic representation illustrating different AF_{local} regions within the grains and at grain boundaries in the AZO-1 film. The gray rectangular boxes represented the columnar-shaped ZnO:Al grains as observed in a. The gaps in between represent the grain boundaries and the colored planes, the Al-dopant layers. These correspond to the iso-concentration surfaces in b. The grid-shaped patterns within the planes represent a high density of Al atoms at the grain boundaries, and they correspond to the iso-concentration surfaces in c. AF_{local} is above 3% in the cross-shape patterns and between 1.7% and 3% in the colored planes. Two-dimensional concentration maps of the three layers shown in b and c are given in the Supporting Information (Figure S2).

into the film by a single ALD cycle that has a growth rate of 0.1 nm/cycle. Compared to this width of 0.1 nm, the fwhm of 2 nm represents a significant broadening of the Al-dopant layers. Note that in the upper profile of Figure 2d, an asymmetric peak broadening is observed: more downward broadening than upward. Asymmetric interface profiles in APT data must be treated with caution because local magnification effects can occur when the layers have different evaporation fields, leading to fluctuations in the atomic density and thus reduced fidelity of spatial position.[24,25] However, in the case of the current measurements, the density fluctuations in the 1D profile are such that there is an apparent higher atomic density on the interface going from the AlO_x layer (higher evaporation field) to ZnO (lower evaporation field). This would, therefore, tend to suppress the perceived downward broadening rather than enhance it.

There are three potential reasons for the measured broadening in the 1D profiles: (*i*) the roughness of the layer and a misalignment from the normal of the sampling volume to each of the surfaces, causing projection effects; (*ii*) the resolution limit of the technique; and (*iii*) an actual vertical spread of the Al atoms in the films.

Option *i* reflects the issues in extracting local compositional information from a sample with a complex 3D geometry. In the samples studied here, the surface topography of all layers within the stacks varies strongly along each interface. For instance, the volume of the AZO-2 stack depicted in Figure 2b would not allow for extracting a 20-nm-wide cylindrical volume perpendicular to the interfaces without having significant interface broadening. As mentioned, by taking this into account, the location and size of the 15−20 nm diameter sampling cylinder was chosen based on the shape of the layers to provide a suitable compromise between sharper profiles and sufficient compositional sensitivity. By such careful selection of the subvolumes in the APT data sets, the effect of projected interface broadening was minimized and is expected to be significantly less than 2 nm.

Option *ii* assumes that the limit of the spatial resolution of APT has resulted in broadening of the Al profiles. This resolution is highly specimen dependent. In some publications the depth resolution of APT is reported to be better than 0.4 nm/decade,[26−28] and for some materials, the reconstruction of individual atomic planes is used to demonstrate "atomic" resolution.[27] However, for measurement of compound semiconductors, the field evaporation behavior is often too disordered to achieve such precision. As mentioned before, the broadening of the peaks of the Al-dopant layers in the AZO-1 film is estimated to have an fwhm of 2 nm. By simulating the Al profiles as δ-functions and assuming all the peak broadening is a result of the experimental profile, described by a Gaussian broadening function, we can estimate an upper-bound to this factor (see Supporting Information, Figure S1). From the degree of separation observed in the 1D profile of the AZO-3 film, we can conclude that the contribution of the potential instrument resolution limitation to the peak broadening is narrower than ∼1.5 nm fwhm. This suggests that there must be additional broadening of the peaks other than potential instrument resolution limitations.

Having dismissed measurement and instrumental artifacts to be the sole cause of the broadened Al distribution, option *iii* must be considered, i.e., a physical reason for a vertical distribution of Al dopants. Thermally driven atomic diffusion of Al into a ZnO matrix has been observed in other experiments but appears to be relevant only when the samples are annealed at temperatures higher than 800 °C because of the high activation energy for diffusion of Al in ZnO (E_a = ∼ 2.8 eV).[29,30] Therefore, such atomic diffusion is unlikely to be the reason for the observation of

DOI: 10.1021/acs.chemmater.7b03501
Chem. Mater. 2018, 30, 1209−1217

a significant broadening in the present case, where the substrate stage temperature is only 250 °C. A more likely explanation is the intermixing of Al and Zn atoms that can occur easily via surface reactions during ALD growth.[31] For example, an etching effect has been observed when TMA reacts with a ZnO surface,[14,32,33] i.e., TMA can remove surface Zn atoms, and consequently, Al atoms can occupy the newly vacant surface sites. This etching effect might introduce downward spreading of Al atoms, accounting for the asymmetry of the profile mentioned above.

Reconsidering the typical representation of dopant profiles obtained by ALD supercycles, as shown in Figure 1b, it is clear that for ZnO:Al films the δ-function distribution is indeed strongly idealized. The Al distribution is significantly broadened, and hence, for depositions with low cycle ratios, which result in small spacing between layers of AlO and high doping levels, there will be overlaps of Al profiles. The latter results in a nonzero local Al density throughout the entire stack, as also observed in Figure 2d. The exact shape of the Al density profile will affect both the conductivity[12] as well as the doping efficiency, as will be addressed in the Discussion.

Al Distribution at Grain Boundaries. So far, the discussion has focused on the distribution of Al within the ZnO:Al grains. Yet the ZnO:Al grain size is by no means infinite, and effects introduced by grain boundaries need to be taken into account. Grain boundaries can have a pronounced influence on the electrical transport properties, e.g., by grain boundary scattering. In order to decrease the resistivity of ZnO:Al films, the improvement of the carrier mobility is at least as important as the enhancement of the carrier density. As a matter of fact, it is even preferred to reduce the resistivity by increasing the mobility rather than by increasing the carrier density in cases where free carrier absorption has a negative impact on the functionality of the ZnO:Al, such as in solar cells.[34] The carrier mobility of ITO ranges typically from 20 to 40 $cm^2 V^{-1} s^{-1}$,[35] which is significantly higher than that of ZnO:Al (~10 $cm^2 V^{-1} s^{-1}$).[5,12] A significant limiting factor causing this difference in carrier mobility is grain boundary scattering.[36] This scattering has a minor effect for (Sn-doped) indium oxide due to a low trap density at the grain boundaries (~1.5×10^{12} cm^{-2}) but plays an important role for ZnO:Al due to a high trap density (~3×10^{13} cm^{-2}).[2] Previous work[12] indicates that the Hall mobility of ZnO:Al prepared by ALD is typically 80% of the intragrain mobility. The remaining 20% difference is ascribed to grain boundary scattering. Therefore, it is also relevant to investigate the Al distribution at grain boundaries.

In order to study the Al distribution at grain boundaries, first the morphology of the entire ZnO/ZnO:Al stack was imaged by bright-field TEM, as shown in Figure 3a. Grains with a columnar-growth shape throughout the entire stack were observed. On the basis of this image, the width of the grains is estimated to be ~40 nm. The 3D morphology of the three Al-dopant layers in the AZO-1 film is presented via the APT-derived iso-concentration surfaces of AF_{local} = 1.7% and AF_{local} = 3.0% as shown in Figure 3b and c, respectively. For clarity, these three Al-dopant layers are indicated by different colors. The 1.7% iso-concentration surface provides a 3D representation of the faceted Al-dopant layers shown in the TEM and APT images (Figure 2b and c). The 3.0% iso-concentration surface highlights some regions inside the Al-dopant layer that are found to have a further enhanced Al concentration. The 3.0% iso-concentration surface has a grid-shaped pattern. Especially in the topmost Al-dopant layer, the grid-shaped pattern is more obvious (see also Figure S2) and has a pitch of around 20−30 nm. As a side note, it is important to underline here that these Al distributions are not caused by the APT analysis itself: the consistency in results between measurements with different laser pulse energies suggests that preferential migration and retention of surface atoms by the APT measurements is not responsible for the Al enrichment observed in the grain boundaries.[37]

The correlation between the microstructure of ZnO grains imaged by TEM and the lateral Al distribution measured by APT is schematically represented in Figure 3d. The transparent parts of the colored planes in Figure 3d indicate Al-dopant layers in ZnO grains with 1.7% < AF_{local} < 3.0%, while the grid-shaped patterns indicate Al-dopant layers at grain boundaries with AF_{local} > 3.0%. This can be concluded from the fact that grid-shaped pattern within the planes follows the shape and locations of grain boundaries in the Al-dopant layers, whereas the pitch of the pattern (~30 nm) corresponds with the grain size in the TEM image (~30−40 nm). The columnar shape of the ZnO:Al grains is also consistent with the elongated grains of the entire film stack as shown in Figure 3a.

The formation of the Al enrichment at grain boundaries can hint at grain boundaries acting as trapping centers of Al,[38] although also other effects such as preferred etching of TMA on the ZnO surface at grain boundaries can play a role as well. Such effects can lead to an enrichment of Al at the intersection between the (predominantly vertical) grain boundaries and at the (mostly horizontal) planes where Al atoms are incorporated in the ZnO by the Al_2O_3 ALD cycles. On the other hand, no enrichment of Al is observed in those areas of the grain boundaries in between the Al-dopant layers, suggesting no significant segregation out of the Al-dopant layers.

DISCUSSION

The APT results in the previous section provide a unique insight into the distribution of the Al atoms on the ZnO film matrix. Clearly, the Al atoms are not distributed according a perfect δ-doping profile, while the Al atoms are concentrated at distinct film depths. There is a broadened distribution that can even result in overlapping tails when the spacing between the Al-dopant layers is small, which happens at low values of the cycle ratio, m. Moreover, it has been observed that there is an enrichment of Al atoms at grain boundaries. In the view of the results obtained, the issue with limited doping efficiency will be discussed in this section. In particular, two factors influencing the doping efficiency will be addressed: the solubility limit and the disorder-induced carrier localization.

The solid solubility of Al in the ZnO matrix is relatively low because Zn and Al have different oxidation states, ionic radii, and coordination preferences.[39] The values of the solubility limit reported in the literature vary. For example, a value of AF_{global} = 0.3% is reported for ZnO:Al powders synthesized via the Pechini route and is based on the observation that an additional phase $ZnAl_2O_4$ was detected by X-ray diffraction (XRD) after annealing at very high temperatures (>1000 °C).[39] For ZnO:Al thin films prepared by the sol−gel method[40] or by the spray pyrolysis technique,[41] a degradation of the crystallinity of the ZnO:Al films was observed when AF_{global} > 2%. In these literature reports, AF_{local} was not measured, but it is fair to assume a homogeneous Al distribution for the deposition methods employed (although this might not be fully trivial as shown by a recent study on B-doped ZnO prepared by low-pressure CVD).[42] In the case of the ZnO:Al thin films grown by ALD, a decrease of crystallinity was observed when AF_{global} > 3%.[43] This value is also in line with the current results in which the grains become heavily disrupted

DOI: 10.1021/acs.chemmater.7b03501
Chem. Mater. 2018, 30, 1209−1217

when going from AZO-1 to AZO-3 (see Figure 3). Even for AZO-1 with AF_{global} = 1.9%, the Al-dopant layers have disrupted the ZnO grains (see also TEM images in ref 12). The value of AF_{global} = 1.9% for AZO-1 corresponds with AF_{local} values up to ∼4% as shown in Figure 2.

The corresponding Al−Al interatomic distance (d_{sol}) at the solubility limit can be approximated by

$$d_{sol} \approx \sqrt[3]{n_{Al,sol}} \quad (2)$$

after calculating $n_{Al,sol}$ from AF_{local} using the atomic density of Zn in undoped ZnO. On the basis of the solubility limit values mentioned above ($0.3\% \leq AF_{local} \leq 4\%$), the corresponding value of d_{sol} is between 0.9 and 2.2 nm. When the local Al density is below the solubility limit ($n_{Al} < n_{Al.sol}$ and $d_{Al-Al} > d_{sol}$), the Al atoms can be substitutionally incorporated in the Zn positions in the ZnO matrix and effectively act as electron donors. When the local Al density is above the solubility limit ($n_{Al} > n_{Al.sol}$ and $d_{Al-Al} < d_{sol}$), a fraction of the Al atoms may form AlO_x clusters or $ZnAl_2O_4$ compounds or segregate to the grain boundaries. These Al atoms are unlikely to act as electron donors. Therefore, the doping efficiency is lower when the local Al density becomes too high.

The reduced doping efficiency at high doping levels can also result from disorder-induced carrier localization. In the literature, it has been reported that intrinsic defects, such as oxygen vacancies (V_O^{2+}),[44,45] and extrinsic defects, such as substitutional dopant atoms at zinc sites (e.g., Ga_{Zn}^{+}),[46] can cause disorder in the ZnO lattice. During electrical transport, electrons can be backscattered by such disorder, leading to the self-interference of coherent electron wave functions.[44] As a result, the scattered electrons are weakly localized, which limits the contribution of the electrons to the conductivity.[46] The inelastic diffusion length (L_{in}) can be expressed by[46]

$$L_{in} = \sqrt{D\tau_{in}} = \sqrt{\hbar D/k_B T} \quad (3)$$

where D is the electron diffusion coefficient, τ_{in} is the inelastic relaxation time, and $\hbar$, k_B, and T are the reduced Planck constant, Boltzmann constant, and absolute temperature, respectively. With increasing doping levels, the lattice disorder increases. When the interatomic distance between dopant impurities is smaller than L_{in}, electrons start to interfere constructively.[46] Applying this theory to the ZnO:Al case, the value of D is ∼0.213 cm^2/s in the ZnO matrix,[46] resulting in L_{in} = ∼0.74 nm at room temperature (T = 298 K). It is reasonable to propose that when the interatomic distance of Al is smaller than L_{in}, i.e., d_{Al-Al} < ∼0.74 nm, weak localization of electrons will become significant. These weakly localized electrons may not (fully) contribute to the carrier density measured by the Hall measurements and hence negatively affect the calculated doping efficiency.

In summary, the Al−Al interatomic distance at the solubility limit (d_{sol}) and the inelastic diffusion length are both on the order of ∼1 nm. Therefore, to obtain a high doping efficiency, an Al−Al interatomic distance d_{Al-Al} > ∼1 nm is desired, which corresponds to a local Al density n_{Al} < ∼1 nm^{-3}, i.e., AF_{local} < ∼2.5%. The measured Al concentrations in the three profiles displayed in Figure 2d appear to exceed this doping level, either over the full thickness of the stack (AZO-3) or locally (AZO-1 and AZO-2). This indicates that at the positions where ALD Al_2O_3 cycles are inserted during film growth, the density of incorporated Al atoms is too high to obtain an optimal conductivity and doping efficiency. On the other hand, the aforementioned broadening of the Al profiles has a beneficial effect on the doping efficiency in the AZO-1 and AZO-2 stacks, as a smaller fraction of the Al contributes to cluster formation than in the case of a δ-doped layer. In order to achieve a higher doping efficiency, the amount of Al atoms incorporated during one ALD Al_2O_3 cycle should be reduced. This hypothesis is supported by other experiments, described in refs 14 and 15 where it was found that deposition processes that reduce the number of incorporated Al atoms give rise to a significant enhancement of doping efficiency.

CONCLUSIONS

In this work, the Al distribution in ALD-prepared ZnO:Al films and its effect on doping efficiency have been investigated. The 3D spatial distribution of Al in the ZnO:Al thin films has been examined on an atomic scale using the combination of TEM and APT. It has been found that the ZnO:Al films are characterized by layers with a high local Al concentration. These layers are not δ-layers but rather exhibit a vertical concentration profile, which causes overlapping of the Al distributions of adjacent Al-dopant layers. Because of the solubility limit of Al in ZnO and the disorder-induced carrier localization, a high local Al density will result in a low doping efficiency. In addition, an enrichment of Al at grain boundaries is observed at intervals corresponding to layers where Al atoms are incorporated. Such a better understanding of the correlation between growth parameters, atomic distribution, and electrical performance can prove to be helpful for future optimizations of the film resistivity of TCOs prepared by ALD.

ASSOCIATED CONTENT

Supporting Information

The Supporting Information is available free of charge on the ACS Publications website at DOI: 10.1021/acs.chemmater.7b03501.

Simulated one-dimensional Al fractions in the ZnO:Al films and two-dimensional color maps of the iso-concentration surfaces of Al in the ZnO:Al film AZO-1 (PDF)

AUTHOR INFORMATION

Corresponding Author

*E-mail: w.m.m.kessels@tue.nl.

ORCID

Bart Macco: 0000-0003-1197-441X

Wilhelmus M. M. Kessels: 0000-0002-7630-8226

Notes

The authors declare no competing financial interest.

ACKNOWLEDGMENTS

The authors thank Holst Centre/IMEC-NL, The Netherlands, for financially supporting this project. This research has also received funding from the European Union's Horizon 2020 research and innovation programme under grant agreement No. 641864 (INREP). The funding of the atomic resolution TEM facility by the Dutch province of Noord-Brabant as well as the fruitful discussions with Dr. A. Illiberi (TNO) and Prof. Dr. P. Koenraad (Eindhoven University of Technology) are gratefully acknowledged. The research of W.M.M.K. has been made possible by the Dutch Technology Foundation STW and The Netherlands Organization for Scientific Research (NWO, VICI program).

DOI: 10.1021/acs.chemmater.7b03501
Chem. Mater. 2018, 30, 1209−1217

REFERENCES

(1) Hosono, H.; Ohta, H.; Orita, M.; Ueda, K.; Hirano, M. Frontier of Transparent Conductive Oxide Thin Films. *Vacuum* **2002**, *66* (3−4), 419−524.

(2) Ellmer, K.; Mientus, R. Carrier Transport in Polycrystalline ITO and ZnO: Al II: The Influence of Grain Barriers and Boundaries. *Thin Solid Films* **2008**, *516* (17), 5829−5835.

(3) Nomura, K.; Ohta, H.; Takagi, A.; Kamiya, T.; Hirano, M.; Hosono, H. Room-Temperature Fabrication of Transparent Flexible Thin-Film Transistors Using Amorphous Oxide Semiconductors. *Nature* **2004**, *432* (7016), 488−492.

(4) Fortunato, E.; Ginley, D.; Hosono, H.; Paine, D. C. Transparent Conducting Oxides for Photovoltaics. *MRS Bull.* **2007**, *32* (March), 242−247.

(5) Minami, T. Transparent Conducting Oxide Semiconductors for Transparent Electrodes. *Semicond. Sci. Technol.* **2005**, *20* (4), S35−S44.

(6) George, S. M. Atomic Layer Deposition: An Overview. *Chem. Rev.* **2010**, *110* (1), 111−131.

(7) Profijt, H. B.; Potts, S. E.; van de Sanden, M. C. M.; Kessels, W. M. M. Plasma-Assisted Atomic Layer Deposition: Basics, Opportunities, and Challenges. *J. Vac. Sci. Technol., A* **2011**, *29* (5), 50801.

(8) Lee, D.-J.; Kim, H.-M.; Kwon, J.-Y.; Choi, H.; Kim, S.-H.; Kim, K.-B. Structural and Electrical Properties of Atomic Layer Deposited Al-Doped ZnO Films. *Adv. Funct. Mater.* **2011**, *21* (3), 448−455.

(9) Dasgupta, N. P.; Neubert, S.; Lee, W.; Trejo, O.; Lee, J.-R.; Prinz, F. B. Atomic Layer Deposition of Al-Doped ZnO Films: Effect of Grain Orientation on Conductivity. *Chem. Mater.* **2010**, *22* (16), 4769−4775.

(10) Tynell, T.; Karppinen, M. Atomic Layer Deposition of ZnO: A Review. *Semicond. Sci. Technol.* **2014**, *29*, 43001.

(11) Macco, B.; Deligiannis, D.; Smit, S.; van Swaaij, R. A. C. M. M.; Zeman, M.; Kessels, W. M. M. Influence of Transparent Conductive Oxides on Passivation of a-Si:H/c-Si Heterojunctions as Studied by Atomic Layer Deposited Al-Doped ZnO. *Semicond. Sci. Technol.* **2014**, *29* (12), 122001.

(12) Wu, Y.; Hermkens, P. M.; van de Loo, B. W. H.; Knoops, H. C. M.; Potts, S. E.; Verheijen, M. A.; Roozeboom, F.; Kessels, W. M. M. Electrical Transport and Al Doping Efficiency in Nanoscale ZnO Films Prepared by Atomic Layer Deposition. *J. Appl. Phys.* **2013**, *114* (2), 24308.

(13) Yanguas-Gil, A.; Peterson, K. E.; Elam, J. W. Controlled Dopant Distribution and Higher Doping Efficiencies by Surface-Functionalized Atomic Layer Deposition. *Chem. Mater.* **2011**, *23*, 4295−4297.

(14) Wu, Y.; Potts, S. E.; Hermkens, P. M.; Knoops, H. C. M.; Roozeboom, F.; Kessels, W. M. M. Enhanced Doping Efficiency of Al-Doped ZnO by Atomic Layer Deposition Using Dimethylaluminum Isopropoxide as an Alternative Aluminum Precursor. *Chem. Mater.* **2013**, *25* (22), 4619−4622.

(15) Garcia-Alonso, D.; Potts, S. E.; van Helvoirt, C. A. A.; Verheijen, M. a.; Kessels, W. M. M. Atomic Layer Deposition of B-Doped ZnO Using Triisopropyl Borate as the Boron Precursor and Comparison with Al-Doped ZnO. *J. Mater. Chem. C* **2015**, *3* (13), 3095−3107.

(16) Jaramillo, R.; Youssef, A.; Akey, A.; Schoofs, F.; Ramanathan, S.; Buonassisi, T. Using Atom-Probe Tomography to Understand ZnO:Al/SiO2/Si Schottky Diodes. *Phys. Rev. Appl.* **2016**, *6*, 34016.

(17) Wu, Y.; Macco, B.; Vanhemel, D.; Kölling, S.; Verheijen, M. A.; Koenraad, P. M.; Kessels, W. M. M.; Roozeboom, F. Atomic Layer Deposition of In2O3:H from InCp and H2O/O2: Microstructure and Isotope Labeling Studies. *ACS Appl. Mater. Interfaces* **2017**, *9*, 592−601.

(18) Scappucci, G.; Klesse, W. M.; Hamilton, A. R.; Capellini, G.; Jaeger, D. L.; Bischof, M. R.; Reidy, R. F.; Gorman, B. P.; Simmons, M. Y. Stacking of 2D Electron Gases in Ge Probed at the Atomic Level and Its Correlation to Low-Temperature Magnetotransport. *Nano Lett.* **2012**, *12* (9), 4953−4959.

(19) Shimizu, Y.; Takamizawa, H.; Inoue, K.; Yano, F.; Nagai, Y.; Lamagna, L.; Mazzeo, G.; Perego, M.; Prati, E. Behavior of Phosphorus and Contaminants from Molecular Doping Combined with a Conventional Spike Annealing Method. *Nanoscale* **2014**, *6* (2), 706−710.

(20) Thompson, K.; Larson, D. J.; Ulfig, R. Pre-Sharpened and Flat-Top Microtip Coupons: A Quantitative Comparison for Atom-Probe Analysis Studies. *Microsc. Microanal.* **2005**, *11* (Suppl 2), 2004−2005.

(21) Larson, D. J.; Foord, D. T.; Petford-Long, A. K.; Liew, H.; Blamire, M. G.; Cerezo, A.; Smith, G. D. W. Field-Ion Specimen Preparation Using Focused Ion-Beam Milling. *Ultramicroscopy* **1999**, *79* (1−4), 287−293.

(22) Miller, M. K.; Russell, K. F.; Thompson, K.; Alvis, R.; Larson, D. J. Review of Atom Probe FIB-Based Specimen Preparation Methods. *Microsc. Microanal.* **2007**, *13* (6), 428−436.

(23) Kelly, T. F.; Larson, D. J. Atom Probe Tomography 2012. *Annu. Rev. Mater. Res.* **2012**, *42* (1), 1−31.

(24) Vurpillot, F.; Cerezo, A.; Blavette, D.; Larson, D. J. Modeling Image Distortions in 3DAP. *Microsc. Microanal.* **2004**, *10* (3), 384−390.

(25) Larson, D. J.; Geiser, B. P.; Prosa, T. J.; Kelly, T. F. On the Use of Simulated Field-Evaporated Specimen Apex Shapes in Atom Probe Tomography Data Reconstruction. *Microsc. Microanal.* **2012**, *18* (5), 953−963.

(26) Koelling, S.; Gilbert, M.; Goossens, J.; Hikavyy, A.; Richard, O.; Vandervorst, W. High Depth Resolution Analysis of Si/SiGe Multilayers with the Atom Probe. *Appl. Phys. Lett.* **2009**, *95* (14), 144106.

(27) Vurpillot, F.; Da Costa, G.; Menand, A.; Blavette, D. Structural Analyses in Three-Dimensional Atom Probe: A Fourier Transform Approach. *J. Microsc.* **2001**, *203* (3), 295−302.

(28) Shimizu, Y.; Kawamura, Y.; Uematsu, M.; Tomita, M.; Kinno, T.; Okada, N.; Kato, M.; Uchida, H.; Takahashi, M.; Ito, H.; Ishikawa, H.; Ohji, Y.; Takamizawa, H.; Nagai, Y.; Itoh, K. M. Depth and Lateral Resolution of Laser-Assisted Atom Probe Microscopy of Silicon Revealed by Isotopic Heterostructures. *J. Appl. Phys.* **2011**, *109* (3), 36102.

(29) Nakagawa, T.; Sakaguchi, I.; Matsumoto, K.; Uematsu, M.; Haneda, H.; Ohashi, N. Observation of Diffusion Behavior in Al-Implanted ZnO Single Crystal. *Key Eng. Mater.* **2009**, *421−422*, 197−200.

(30) Johansen, K. M.; Vines, L.; Bjørheim, T. S.; Schifano, R.; Svensson, B. G. Aluminum Migration and Intrinsic Defect Interaction in Single-Crystal Zinc Oxide. *Phys. Rev. Appl.* **2015**, *3* (2), 24003.

(31) Knez, M. Diffusion Phenomena in Atomic Layer Deposition. *Semicond. Sci. Technol.* **2012**, *27* (7), 74001.

(32) Na, J.-S.; Scarel, G.; Parsons, G. N. In Situ Analysis of Dopant Incorporation, Activation, and Film Growth during Thin Film ZnO and ZnO: Al Atomic Layer Deposition. *J. Phys. Chem. C* **2010**, *114*, 383−388.

(33) Elam, J.; George, S. Growth of ZnO/Al2O3 Alloy Films Using Atomic Layer Deposition Techniques. *Chem. Mater.* **2003**, *15*, 1020−1028.

(34) Berginski, M.; Hüpkes, J.; Schulte, M.; Schöpe, G.; Stiebig, H.; Rech, B.; Wuttig, M. The Effect of Front ZnO: Al Surface Texture and Optical Transparency on Efficient Light Trapping in Silicon Thin-Film Solar Cells. *J. Appl. Phys.* **2007**, *101* (7), 74903.

(35) De Wolf, S.; Descoeudres, A.; Holman, Z. C.; Ballif, C. High-Efficiency Silicon Heterojunction Solar Cells: A Review. *Green* **2012**, *2* (1), 7−24.

(36) Ellmer, K.; Mientus, R. Carrier Transport in Polycrystalline Transparent Conductive Oxides: A Comparative Study of Zinc Oxide and Indium Oxide. *Thin Solid Films* **2008**, *516* (14), 4620−4627.

(37) Tu, Y.; Takamizawa, H.; Han, B.; Shimizu, Y.; Inoue, K.; Toyama, T.; Yano, F.; Nishida, A.; Nagai, Y. Influence of Laser Power on Atom Probe Tomographic Analysis of Boron Distribution in Silicon. *Ultramicroscopy* **2017**, *173*, 58−63.

(38) Suzuoka, T. Lattice and Grain Boundary Diffusion in Polycrystals. *Trans. Jpn. Inst. Met.* **1961**, *2*, 25−33.

(39) Serier, H.; Gaudon, M.; Ménétrier, M. Al-Doped ZnO Powdered Materials: Al Solubility Limit and IR Absorption Properties. *Solid State Sci.* **2009**, *11* (7), 1192−1197.

(40) Zi-Qiang, X.; Hong, D.; Yan, L.; Hang, C. Al-Doping Effects on Structure, Electrical and Optical Properties of c-Axis-Orientated ZnO: Al Thin Films. *Mater. Sci. Semicond. Process.* **2006**, *9* (1−3), 132−135.

DOI: 10.1021/acs.chemmater.7b03501
Chem. Mater. 2018, 30, 1209−1217

(41) El Manouni, A.; Manjón, F. J.; Perales, M.; Mollar, M.; Marí, B.; Lopez, M. C.; Ramos Barrado, J. R. Effect of Thermal Annealing on ZnO: Al Thin Films Grown by Spray Pyrolysis. *Superlattices Microstruct.* **2007**, *42* (1−6), 134−139.
(42) Lorenzo, F.; Aebersold, A. B.; Morales-Masis, M.; Ledinský, M.; Escrig, S.; Vetushka, A.; Alexander, D. T. L.; Hessler-Wyser, A.; Fejfar, A.; Hébert, C.; Nicolay, S.; Ballif, C. Direct Imaging of Dopant Distribution in Polycrystalline ZnO Films. *ACS Appl. Mater. Interfaces* **2017**, *9*, 7241.
(43) Banerjee, P.; Lee, W.-J.; Bae, K.-R.; Lee, S. B.; Rubloff, G. W. Structural, Electrical, and Optical Properties of Atomic Layer Deposition Al-Doped ZnO Films. *J. Appl. Phys.* **2010**, *108* (4), 43504.
(44) Saha, D.; Das, A. K.; Ajimsha, R. S.; Misra, P.; Kukreja, L. M. Disorder-Driven Carrier Transport in Atomic Layer Deposited ZnO Thin Films. *arXiv Prepr.* **2013**, arXiv:1301.1172
(45) Tiwari, A.; Jin, C.; Narayan, J.; Park, M. Electrical Transport in ZnO 1-δ Films: Transition from Band-Gap Insulator to Anderson Localized Insulator. *J. Appl. Phys.* **2004**, *96* (7), 3827−3830.
(46) Bhosle, V.; Tiwari, A.; Narayan, J. Electrical Properties of Transparent and Conducting Ga Doped ZnO. *J. Appl. Phys.* **2006**, *100* (3), 33713.

DOI: 10.1021/acs.chemmater.7b03501
Chem. Mater. 2018, 30, 1209−1217